Multiple Active Site Histidine Protonation States in *Acetobacter aceti* N^5-Carboxyaminoimidazole Ribonucleotide Mutase Detected by REDOR NMR†

Jacob Schaefer, Hong Jiang, Aaron E. Ransome, and T. Joseph Kappock*

Department of Chemistry, Washington University, St. Louis, Missouri 63130-4899

Received May 11, 2007; Revised Manuscript Received June 18, 2007

ABSTRACT: Class I PurE (N^5-carboxyaminoimidazole mutase) catalyzes a chemically unique mutase reaction. A working mechanistic hypothesis involves a histidine (His45 in *Escherichia coli* PurE) functioning as a general acid, but no evidence for multiple protonation states has been obtained. Solution NMR is a peerless tool for this task but has had limited application to enzymes, most of which are larger than its effective molecular size limit. Solid-state NMR is not subject to this limit. REDOR NMR studies of a 151 kDa complex of uniformly ^{15}N-labeled *Acetobacter aceti* PurE (*Aa*PurE) and the active site ligand [6-^{13}C]-citrate probed a single ionization equilibrium associated with the key histidine (*Aa*PurE His59). In the *Aa*PurE complex, the citrate central carboxylate C6 ^{13}C peak moves upfield, indicating diminution of negative charge, and broadens, indicating heterogeneity. Histidine ^{15}N chemical shifts indicate His59 exists in approximately equimolar amounts of an N$^\delta$-unprotonated (pyridine-like) form and an N$^\delta$-protonated (pyrrole-like) form, each of which is ∼4 Å from citrate C6. The spectroscopic data are consistent with proton transfers involving His59 N$^\delta$ that are invoked in the class I PurE mechanism.

The microbial or class I form of PurE[1] (N^5-carboxyaminoimidazole ribonucleotide mutase) reversibly interconverts N^5-carboxyaminoimidazole ribonucleotide (N^5-CAIR) to 4-carboxy-5-aminoimidazole ribonucleotide (CAIR) in the de novo purine biosynthetic pathway (*1*, *2*). The mechanism proposed for this chemically unique reaction (Scheme 1) includes a decarboxylation−recarboxylation sequence initiated by substrate protonation at the N^5-CAIR carbamate (or CAIR C4) (*3*). One likely enzyme-bound intermediate is 5-aminoimidazole ribonucleotide (AIR) and CO_2, which are the substrates for the animal or class II form of PurE (*4*). Mechanistic investigations of PurE are complicated by nonenzymatic interconversions of AIR, N^5-CAIR, and CAIR, which depend on CO_2/HCO_3^- concentrations, temperature, and pH.

Multiple crystal structures are available for class I PurEs, including several structures of *Escherichia coli* and *Acetobacter aceti* PurE bound to substrates or substrate analogues (*5*, *6*). In the current mechanistic proposal, an essential histidine residue (*E. coli* PurE [*Ec*PurE] His45) performs acid−base chemistry, the carboxylate/CO_2 group occupies a binding pocket defined by backbone amides, and the aminoimidazole ring rotates during the reaction (*7*). However, crystal structures do not report on protonation states or the electronic environment in the active site. Ambiguous electron density for some nucleotide·PurE structures, likely arising from partial substrate occupancy or crystals containing different aminoimidazole forms, has also hampered detailed analysis (*5*, *8*).

Scheme 1: Possible Mechanism for the Reversible Class I PurE-Mediated Conversion of N^5-CAIR to CAIR[a]

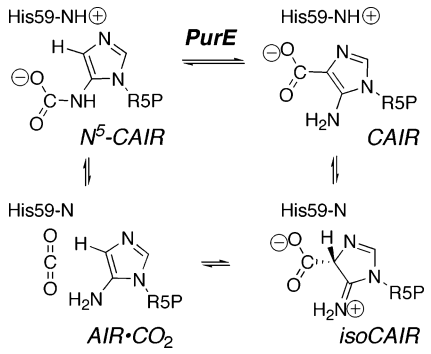

[a] R5P is ribose 5′-phosphate.

A. aceti PurE (*Aa*PurE) was first crystallized with citrate bound to the active site (PDB entry 1u11), interacting principally with His59 ND1 (central carboxylate), Asp33 OD2 (*pro-R* carboxylate), and Gly29 O (*pro-S* carboxylate) (*6*). The first two residues are important in nucleotide binding and catalysis (equivalent to *Ec*PurE His45 and Asp19). Citrate also interacts with two waters that are found in all unliganded PurE structures and that occupy the oxygen atom

† We gratefully acknowledge support from the Herman Frasch Foundation for Research in Agricultural Chemistry (Grant 531-HF02 to T.J.K.), the National Institutes of Health (Grant EB001964 to J.S.), and the National Science Foundation (CAREER Award MCB-0347250 to T.J.K.). Mass spectrometry was provided by the Washington University Mass Spectrometry Resource with support from the NIH National Center for Research Resources (P41RR0954).

* To whom correspondence should be addressed. Telephone: (314) 935-8241. Fax: (314) 935-4481. E-mail: kappock@wustl.edu.

[1] Abbreviations: *Aa*CSH6, citrate synthase from *A. aceti* with a C-terminal hexahistidine tag; *Aa*PurE, PurE from *A. aceti*; AIR, 5-aminoimidazole ribonucleotide; CAIR, 4-carboxy-5-aminoimidazole ribonucleotide; CoA, coenzyme A; ESI-MS, electrospray ionization mass spectrometry; LB, Luria-Bertani medium; LDH, lactate dehydrogenase; N^5-CAIR, N^5-carboxyaminoimidazole ribonucleotide; PEG, poly(ethylene glycol); PEP, phosphoenolpyruvate; PEPC, phosphoenolpyruvate carboxylase (EC 4.1.1.31); PurE, N^5-CAIR mutase (class I, EC 5.4.99.18) or AIR carboxylase (class II, EC 4.1.1.21); REDOR, rotational-echo double-resonance; TPPM, two-pulse phase modulation.

10.1021/bi700899q CCC: $37.00
Published on Web 07/27/2007

positions used by the substrate carboxylate (and CO_2 intermediate) in its binding pocket (*7*). Slightly different citrate positions were observed in the two subunits that make up the asymmetric unit (*8*). While citrate has little resemblance to PurE substrates, it has excellent electron density in complex structures, is stable over a range of pH, and induces fluorescence changes in *Aa*PurE that have been used to determine binding constants for a series of active site mutants (*8*).

The rotational-echo double-resonance (REDOR) NMR experiment detects heteronuclear dipolar interactions (*9*, *10*) and can be used to obtain interatomic distances in appropriately labeled samples (*11*). Here REDOR is used to study a complex of [6-^{13}C]citrate and uniformly ^{15}N-labeled *Aa*PurE ([U-^{15}N]*Aa*PurE). Chemical shifts indicate at least two binding modes for citrate associated with a mixture of N^{δ} protonation states for the key active site histidine, confirming and extending prior crystallographic observations.

EXPERIMENTAL PROCEDURES

Materials and Methods. *A. aceti* citrate synthase with a hexahistidine affinity tag (*Aa*CSH6) was purified as described previously (*12*). Plasmid pJK174 produces both *Aa*PurK and *Aa*PurE, the latter with an extra N-terminal methionine (*8*). Uniformly ^{15}N-labeled *Aa*PurE was purified as described from pJK174/BL21(DE3) cells (8.7 g) induced for 4 h with 0.4 mM IPTG in M9 medium supplemented with 55 mM $^{15}NH_4Cl$ (3 g/L), 15 mM glucose, 2 mM $MgSO_4$, 0.1 mM $CaCl_2$, 0.1 mM $ZnCl_2$, 9 μM $FeCl_3$, 4 μM biotin, 3 μM thiamine·HCl, and 0.2 g/L yeast extract. Aliquots of pure *Aa*PurE (9 mg/mL; 0.5 mM subunit in 10 mM Tris·HCl, pH 8) were stored at −80 °C until they were used. Chemicals and other enzymes were obtained from Aldrich or Sigma. For all enzymes, a unit is defined as the amount forming 1 μmol of product/min.

Analytical Procedures. Solution NMR spectra were recorded using a Mercury 300 spectrometer at 300 MHz (^{1}H) or 75 MHz (^{13}C) and referenced to CH_3OH. Compounds were analyzed using a Waters HPLC system with a Symmetry C18 column (4.6 mm × 75 mm, 3.5 μm) equilibrated with 95% mobile phase A (15 mM KH_2PO_4 in H_2O) and 5% mobile phase B (methanol) running at 0.5 mL/min. These conditions were maintained for 2 min following the injection of each sample. The amount of B was then increased from 5 to 80% over 12 min, maintained at 80% for 6 min, and then returned to 5% B over 5 min. Electrospray ionization mass spectrometry (ESI-MS) was used to determine the degree of incorporation of ^{15}N into purified [U-^{15}N]*Aa*PurE. Protein concentrations were determined using the Bradford method with crystalline bovine serum albumin as a standard (*13*).

The conversion of phosphoenolpyruvate (PEP) to oxaloacetate (OAA) and citrate was monitored by adding a synthetic mixture aliquot (10 μL) to a cuvette containing 50 mM imidazole·HCl (pH 7.6), 120 mM KCl, 60 mM $MgSO_4$, 5 mM NAD, 40 mM ADP, 2 units of lactate dehydrogenase (LDH), and 2 units of pyruvate kinase (PK) in a final volume of 0.5 mL at 25 °C. The synthetic mixture aliquot, NAD, ADP, LDH, and PK were added in that order to the buffer components. The absorbance at 340 nm ($\Delta\epsilon = 6.2$ mM^{-1} cm^{-1}) was measured prior to the addition of LDH, 10 min after addition of LDH, and 10 min after the addition of PK. Pyruvate was quantitated using the difference in the first two absorbance measurements, and PEP was quantitated using the difference in the second and third absorbance measurements.

Synthesis of Ammonium [6-^{13}C]Citrate. The cyclohexylammonium salt of [1-^{13}C]PEP was prepared from sodium [1-^{13}C]pyruvate as described previously (*14*). Each citrate synthesis reaction mixture (4 mL) initially contained 50 mM Tris·HCl (pH 8), 65 mM KCl, 8 mM $NaHCO_3$, 6 mM $MgCl_2$, 4 mM [1-^{13}C]PEP, 2.5 mM acetyl-CoA, 0.5 mM EDTA, 4 units of PEP carboxylase (PEPC), and 32 units of *Aa*CSH6 at 25 °C. After incubation for 24 h, solids were removed by brief centrifugation, and 16 μmol of $NaHCO_3$, 4 units of PEPC, and 32 units of *Aa*CSH6 were added to each mixture. After an additional 12 h, solids were removed and 2 units of PEPC and 32 units of *Aa*CSH6 were added. After a final 24 h, solids were removed by brief centrifugation, macromolecules were removed by being passed through a Centricon YM-10 ultrafiltration device (Amicon), and the solution was adjusted to pH 1−2 (pH paper) using 3 M H_2SO_4. After liquid−liquid extraction against ether (4 days), solvents were removed in vacuo, and the residue was dissolved in H_2O (4 mL) and adjusted to pH 7−8 with NaOH (pH paper). This solution was applied to a Q-Sepharose Fast Flow column (1.5 cm × 5 cm) equilibrated in water adjusted to pH 10 with NaOH. The column was developed with pH 10 NaOH (50 mL) and then a linear gradient of Na_2SO_4 (0 → 0.1 M in pH 10 NaOH, 100 × 100 mL). Fractions containing citrate (located with an $FeCl_3$ colorimetric assay and then confirmed by HPLC and ^{13}C NMR analysis) were pooled, adjusted to pH 1−2 with 3 M H_2SO_4, and subjected to liquid−liquid extraction (4 days) against ether. The residue was taken up in 1 M NH_4OH (10 mL) and dried under vacuum. The residue was dissolved in H_2O (2 mL) and analyzed (12% overall yield from [1-^{13}C]pyruvate): ^{13}C NMR (75 MHz, D_2O) δ 182.25 (6-^{13}C); analytical HPLC $t_{R,citrate} = 1.5$ min; ESI-MS expected for $^{13}C_1C_5H_8O_7$ (M − H) 192.03, observed 192.02.

The Q-Sepharose column and Na_2SO_4 elution was repeated with buffers containing NH_4OH at pH 10, and the dried product was taken up in H_2O (2 mL, pH 8 by pH paper). The area of a HPLC peak at 215 nm was compared to standards to determine the citrate concentration (1.4 mM, 2.8 μmol). The solution was stored at −80 °C.

Sample Preparation. To a solution at 4 °C containing 0.47 mM ammonium [6-^{13}C]citrate, 5 mM HEPES·NaOH (pH 7.4), 0.3125% (w/v) PEG 8000, 15 mM trehalose, 0.67 mg/mL dextran (81.5 kDa), and 0.67 mg/mL dextran (488 kDa) in a 50 mL Falcon tube were slowly added with gentle mixing 0.22 mM [U-^{15}N]*Aa*PurE and 4 mM Tris·HCl (pH 8) (final concentrations given). This solution (6 mL) was frozen in a shell in a liquid N_2 bath and then lyophilized. The sample contained 1.3 μmol of [U-^{15}N]*Aa*PurE (24 mg) and 2.8 μmol of ammonium [6-^{13}C]citrate (1.5 mg).

REDOR NMR. Spectra for the *Aa*PurE·citrate complex were recorded using a six-frequency transmission-line probe (*15*), having a 12 mm long, 6 mm inside diameter analytical coil and a Chemagnetics/Varian magic-angle spinning ceramic stator. Lyoprotected samples were spun in thin-wall Chemagnetics/Varian 5 mm outside diameter zirconia rotors, with active control of the speed to within ±2 Hz. The

spectrometer was controlled by a Tecmag Libra pulse programmer. Radiofrequency pulses for ^{13}C (125 MHz) and ^{15}N (50.3 MHz) were produced by 2 kW American Microwave Technology power amplifiers. Proton (500 MHz) radiofrequency pulses were generated by a 2 kW Amplifier Systems tube amplifier driven by a 50 W American Microwave Technology power amplifier. The π-pulse lengths were 8 μs for ^{13}C and 9 μs for ^{15}N. The amplitudes of all pulses were under active control (*16*). REDOR dephasing pulses followed the xy-8 phase cycling scheme (*17*). A 12 T static magnetic field was provided by an 89 mm bore Magnex superconducting solenoid. Proton−carbon cross-polarization magic-angle spinning transfers were made with radiofrequency fields of 62.5 kHz. Proton dipolar decoupling was 100 kHz during the acquisition of data. TPPM modulation (*18*) of the proton radiofrequency was generated by an external device running asynchronously with respect to the pulse programmer clock. REDOR spectra were acquired on an alternate scan basis, first S then S_0.

RESULTS

Synthesis of [6-^{13}C]Citrate. [1-^{13}C]PEP was chemically synthesized (48% yield by enzymatic PEP assay) and converted in a one-pot reaction to [1-^{13}C]OAA and then [6-^{13}C]citrate by the sequential actions of PEPC and *Aa*CSH6, using conditions suitable for PEPC and OAA accumulation (*22*, *23*). Trial reactions followed by HPLC were used to find conditions that minimize the slow formation of pyruvate, up to ~10% of the original PEP concentration, while conserving acetyl-CoA (the limiting reagent) and PEPC. Pyruvate coeluted with citrate on anion exchange columns at pH 2, but not at pH 10. [6-^{13}C]Citrate was isolated in 5% overall yield from [1-^{13}C]pyruvate.

Characterization of [U-^{15}N]AaPurE. The efficiency of incorporation of ^{15}N into [U-^{15}N]*Aa*PurE was assessed by ESI-MS. A deconvoluted mass of 19 091 ± 2 Da was obtained, a value 225 Da larger than the values expected for natural isotopic abundance *Aa*PurE (18 865.8 Da) (*8*), which includes natural abundance ^{15}N (0.365%). The observed mass corresponds to a ^{15}N content of 97.2% in each $C_{828}H_{1356}N_{232}O_{253}S_8$ subunit, indicating that little ^{14}N was incorporated from yeast extract present in the growth medium.

$^{13}C\{^{15}N\}$ REDOR. The carbonyl carbon region of the full-echo (S_0) ^{13}C NMR spectrum of the *Aa*PurE·citrate complex after dipolar evolution for 2.56 ms is shown in Figure 1 (bottom, black). The dominant signals arise from the natural abundance ^{13}C of the protein. The vast majority of these carbons are directly bonded to ^{15}N, so their contributions to the dephased-echo spectrum (S) have been removed (Figure 1, top, black). Only two peaks of approximately equal integrated intensity remain. The low-field peak (182 ppm) is assigned to free citrate and the high-field peak (174 ppm) to bound citrate. These chemical shifts indicate that free citrate is charged and the bound citrate is predominantly protonated or hydrogen bonded (*24*). Approximately 60−65% of the bound citrate signal is removed in a $^{13}C\{^{15}N\}$ REDOR experiment with 15.36 ms of dipolar evolution (Figure 1, top, red). Assuming that the REDOR dephasing arises from a single proximate ^{15}N, the C−N dipolar coupling is 60 Hz and the internuclear distance is 3.5 Å.

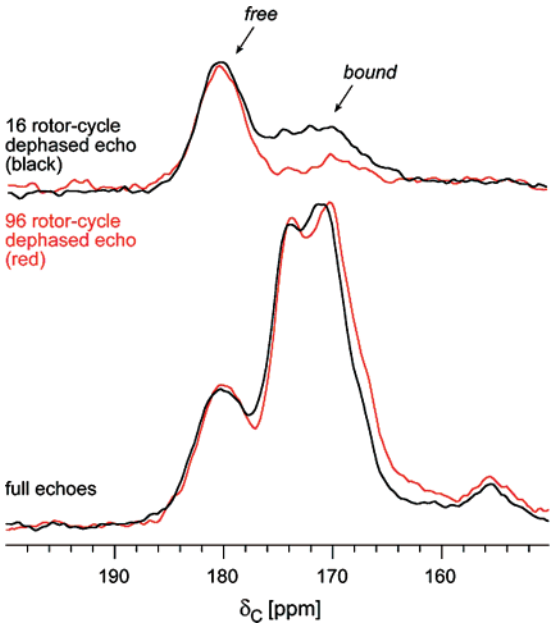

FIGURE 1: Carbonyl region $^{13}C\{^{15}N\}$ REDOR NMR spectra of the *Aa*PurE·citrate complex after dipolar evolution for 2.56 (black) and 15.36 ms (red). The full-echo spectra (scaled to compensate for homogeneous decay) are shown at the bottom of the figure and the dephased echoes at the top. The peaks at 155 ppm and between 171 and 175 ppm arise from natural abundance ^{13}C in [U-^{15}N]-*Aa*PurE, and these are totally dephased (reduced to zero intensity) after 2.56 ms by directly bonded ^{15}N. The two remaining peaks are assigned to ^{13}C label in free (180 ppm) and bound (172 ppm) citrate. The latter undergoes ~60% dephasing after 15.36 ms, consistent with a 3.5 Å $^{13}C-^{15}N$ intermolecular distance. Magic-angle spinning was at 6250 Hz.

$^{15}N\{^{13}C\}$ REDOR. The full-echo ^{15}N NMR spectrum of the complex after dipolar evolution for 16.64 ms shows resolved peaks for lysine, arginine, and histidine side chain nitrogens (Figure 2, bottom). The dominant peak at 95 ppm arises from peptide nitrogens. Spinning sidebands of this peak appear at −55 and 240 ppm. The intensity of the protonated (pyrrole-like, >NH) histidine−nitrogen peak (150 ppm) is ~3 times greater than that of the unprotonated (pyridine-like, ≥N) histidine−nitrogen peak (220 ppm), indicating that two of the four histidines in *Aa*PurE are fully protonated. The REDOR difference spectrum ($\Delta S = S_0 - S$) shows dephasing for all types of nitrogens (Figure 2, top). Much of the dephasing arises from the proximity of ^{15}N to natural abundance ^{13}C and varies from 1% for the lysyl amine peak to ~8% for the peptide amide peak. The dephasing for the two histidine peaks is substantially greater, however, presumably the result of dipolar coupling to the bound citrate ^{13}C label. If we assume that four-fifths of the 20% dephasing of the 220 ppm peak is due to the N^{δ}−citrate label interaction (and the remaining one-fifth to coupling of other pyridine-like ^{15}N to natural abundance ^{13}C), then the $^{15}N^{\delta}-^{13}C$ dipolar coupling for the bound citrate is ~35 Hz and the internuclear distance is 4 Å.

DISCUSSION

Class I PurE catalyzes a unique, intramolecular CO_2 migration reaction. A structure-based mechanistic proposal has the aminoimidazole moiety of AIR rotating within a ternary PurE·CO_2·AIR complex, while the protein remains largely immobile (*7*). Crystal structures of the class I PurE

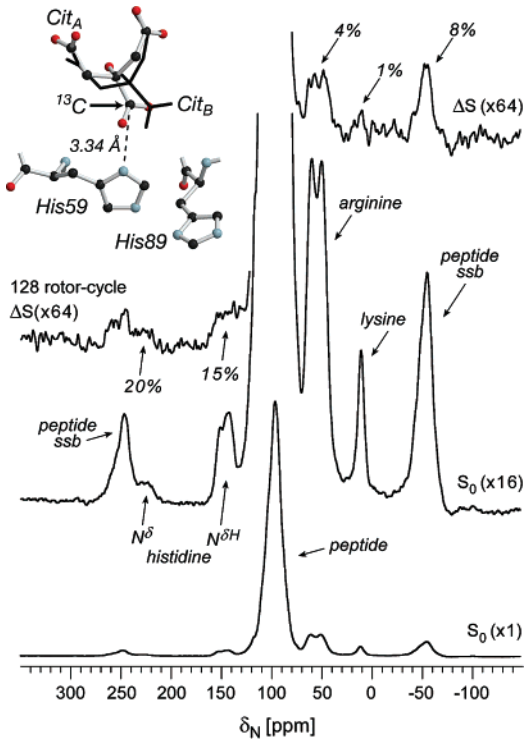

FIGURE 2: ^{15}N{^{13}C} REDOR NMR spectra of the *Aa*PurE·citrate complex after dipolar evolution for 17.92 ms. Full-echo spectra (S_0) are shown at the bottom and middle of the figure, and the REDOR difference ($\Delta S = S_0 - S$, where S is the dephased-echo spectrum) is shown at the top. The histidine nitrogen peaks at 150 and 220 ppm have much more dephasing ($\Delta S/S_0$ expressed as percentages) than other side chain peaks, consistent with the proximity of the citrate ^{13}C label to His59 (inset). The chemical shift scale is relative to external solid ammonium sulfate. (To convert to the chemical shift scale more commonly used in protein NMR, which is referenced to the ^{15}N frequency of liquid ammonia (*32*), add 24 ppm to the values given.) Magic-angle spinning was at 8000 Hz. The inset shows a depiction of superimposed active sites A and B from the *Aa*PurE·citrate complex crystal structure (PDB entry 1u11) showing the two different citrate locations. Subunit A is depicted in ball-and-stick representations, and subunit B is depicted as thick black lines. The subunit A ^{15}N−^{13}C distance is 3.34 Å, and the subunit B ^{15}N−^{13}C distance is 3.53 Å. Structure superposition was performed using all backbone atoms in SwissPDB Viewer (*19*). The drawing was rendered with Molscript (*20*) and Raster3D (*21*).

forms *Ec*PurE and *Aa*PurE show few differences as active site ligands, pH, or individual side chains are altered (*5*, *7*, *8*), indicating the protein is comparatively rigid. Known enzymological differences between *Ec*PurE and *Aa*PurE are minor, but different complexes crystallize for each form (*7*, *8*). *Aa*PurE is the more stable protein, as anticipated because *A. aceti* is an acidophile that maintains an acidic cytoplasm (*25*). Acid shortens the lifetime of the PurE substrates, especially N^5-CAIR, and might affect *Aa*PurE in some as-yet-unknown way.

The serendipitously discovered interaction of *Aa*PurE with citrate is too weak for an in vivo role (*8*). However, investigations of the *Aa*PurE−citrate interaction are useful test cases for comparable spectroscopic studies with the chemically unstable and commercially unavailable aminoimidazole PurE substrates and substrate analogues. Citrate is bound in different orientations in adjacent active sites that would otherwise be related by a 2-fold crystallographic axis. The active sites bracket a stack of four conserved histidines (His59, His89, His89′, and His59′, where the prime indicates a residue from subunit B) (*6*). In both subunits, citrate interacts with two placeholder water/hydroxide molecules that are displaced by the carboxylate moiety in the substrate/product and by CO_2 in postulated intermediates (*7*). In subunit A of the *Aa*PurE·citrate structure (PDB entry 1u11), HOH688 is 2.75 Å from the O7 atom of the citrate hydroxyl and HOH691 is 2.48 Å from the O6 atom of the central carboxylate. In subunit B, HOH682 is 2.46 Å from the O7 atom of the citrate hydroxyl and HOH692 is 2.62 Å from the O6 atom of the central carboxylate. These ligands could carry a net negative charge, since this region functions as a carboxylate binding pocket. Subunit A could then contain citrate with an anionic central carboxylate interacting with a nearby water (HOH691), while subunit B would contain a hydroxide anion (HOH682) interacting with the nearby citrate alcohol. In either case, the hydrogen bonding pattern in the vicinity of His59 is likely to be different in the two orientations.

His59 is not required for citrate binding (*8*). His59 (wild type), Asn, Asp, Phe, and Gln mutants bind citrate at pH 5.3, while Ala and Ser mutants do not (K_d > 10 mM). Comparisons are difficult because at least one of these mutants, H59N-*Aa*PurE, binds citrate in a rather different third orientation.[2]

A direct electrostatic interaction between the citrate central carboxylates, which are separated by ~16 Å, appears unlikely to be responsible for desymmetrizing the citrate binding sites. Citrate orientations A and B appear to differ because of asymmetric His59 and His59′ protonation at each end of the histidine stack, which might electrostatically link adjacent active sites (*6*) but is not essential for activity (*8*). (Alteration of the nearby His89 to chemically dissimilar residues does not profoundly affect enzymatic function or citrate binding.) We anticipated that solution ^{1}H NMR studies of His59 would be difficult to execute on the octameric *Aa*PurE complex (151 kDa) because of its rotational correlation time. However, solid-state NMR is a good option for *Aa*PurE; because of its small subunit size, a high concentration of active sites can be reached, and because subunits adopt essentially identical configurations (*5*−*8*, *26*), heterogeneity in the *Aa*PurE−citrate interaction can be attributed to multiple citrate binding modes.

The change in the ^{13}C chemical shift of bound citrate to high field indicates shielding by the protein (*24*), a change in chemical environment that is likely due to protonation or hydrogen bonding. Multiple conformations or electronic environments are required to account for the broad appearance of the bound signals. While it is difficult to define the pH of lyophilized samples, a free-citrate chemical shift at

[2] Citrate binds in a third orientation to H59N-*Aa*PurE. Citrate is found in half of the active sites in crystal structures determined in either the absence (PDB entry 2fw6) or presence of a nucleotide (PDB entry 2fwp) at pH 5.4. In this third orientation, the citrate *pro-S* carboxylate interacts with Asp33, replacing the *pro-R* carboxylate in the wild-type structure (PDB entry 1u11), while the oxygen atoms of the *pro-R* carboxylate replace the placeholder waters. The alcohol oxygen and the central carboxylate carbon remain in the same place as in orientation A, with the rest of the molecule reorienting by ~120°. For both H59N-*Aa*PurE structures, citrate is bound at full occupancy (in half of the subunits) and has excellent electron density and, therefore, could give insight into the design of inhibitors that target the carboxylate/CO_2 binding site.

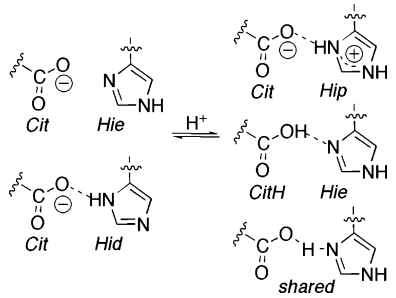

FIGURE 3: Potential interactions between citrate and His59 in the *Aa*PurE·citrate complex, with (right) or without (left) protonation. Atoms labeled C and N contain either ^{13}C or ^{15}N. Abbreviations: Cit, citrate with a deprotonated central carboxylate; CitH, citrate with a protonated central carboxyl; Hid, N^{δ}-protonated His59; Hie, N^{ϵ}-protonated His59; Hip, fully protonated (imidazolium) form of His59. Both Hid and Hip would be consistent with a $^{15}N^{\delta}$ peak at 150 ppm. Hie gives a $^{15}N^{\delta}$ peak at 220 ppm. A single AaPurE·citrate complex is excluded by dephasing by nearby ^{13}C of two separate ^{15}N peaks assigned to different states of His59 N^{δ}. Crystallographically determined (PDB entry 1u11) interatomic distances from His59 N^{δ} to the nearest citrate carboxylate O atom are 2.47 (subunit A) and 2.56 Å (subunit B). Since both dephased ^{15}N peaks overlap with other His side chain ^{15}N peaks, there is no evidence for an unusual electronic environment associated with the "shared" hydrogen bonding interaction illustrated, where the proton is located near the center of the hydrogen bond.

>180 ppm is consistent with a prelyophilization pH higher than 4.28 (*24*). At the slightly basic pH used to form the [U-^{15}N]*Aa*PurE·[6-^{13}C]citrate complex, the central carboxylate should be fully ionized (*27*). While a fully protonated central carboxylate (CitH in Figure 3) cannot be ruled out by these data, it seems more likely that the local hydrogen bonding environment accounts for the upfield ^{13}C shift of bound citrate.

Lysine, arginine, amide (backbone/carboxamide), and histidine ^{15}N peaks are well-resolved from each other. The four histidines present in *Aa*PurE contribute signals at 150 and 220 ppm, corresponding to imidazole ^{15}N bound to pyrrole-like (>NH) and pyridine-like (≥N) nitrogens, respectively. (Both imidazolium cation NH groups appear at 150 ppm.) These peaks are usually imidazole $>N^{\epsilon}H$ and $\geq N^{\delta}$, respectively, although the reverse protonation pattern also occurs (*28*). The $^{15}N\{^{13}C\}$ REDOR spectra indicate [6-^{13}C]citrate interacts mainly with a nearby histidine (Figure 2 inset, His 59; other histidine nitrogens are more than 7 Å distant). Considering the $^{15}N^{\epsilon}-^{13}C$ distance of >5 Å (*6*) and the $1/r^3$ dependence of dipolar coupling, ^{13}C dephasing of the proximal $^{15}N^{\delta}$ would be 4-fold greater (orientation A; 3-fold greater in orientation B) than that of the distal $^{15}N^{\epsilon}$ in the *Aa*PurE·citrate complex (PDB entry 1u11). Instead, the observed dephasing is approximately equal for both pyrrole-like and pyridine-like nitrogens, which is geometrically inconsistent with dephasing from two nitrogens within a single histidine. The most likely explanation is that citrate interacts with an ~1:1 mixture of differently protonated His59 forms.

*Aa*PurE His59 (*Ec*PurE His45) is a key active site acid/base residue, beginning each turnover in the fully protonated (imidazolium) form and delivering a proton to facilitate C−C or C−N bond scission (Scheme 1). The REDOR data indicate that citrate binds to *Aa*PurE near a His59 side chain that adopts a near-equimolar mixture of pyrrole- and pyridine-like protonation states, consistent with the different citrate orientations observed in prior crystallographic studies (*6*). In crystals, His59 is always oriented with N^{δ} nearest the substrate binding site. Thus, the observed pyrrole-like (>NH) contact could represent His59 imidazolium configuration Hip or imidazole configuration Hid (Figure 3). The pyridine-like (≥N) contact must be imidazole configuration Hie. Assuming the central citrate carboxylate is anionic, the latter contact identifies the Cit−Hie pair as being in the *Aa*PurE·citrate complex. These data also exclude a single configuration, or exchange of multiple conformations that is rapid on the NMR time scale, involving a "shared" proton (Figure 3), analogous to aspartate−histidine interactions observed in solution NMR studies of small proteases (*29*−*31*).

We propose that the pyrrole-like contact mainly detects imidazolium configuration Hip, which integrated peak areas indicate is present in half of the *Aa*PurE histidines. (The alternate interpretation of the pyrrole-like contact would suggest that *Aa*PurE maintains a near-equimolar level of each His59 imidazole tautomer, which is unnecessary in the proposed mechanism and unlikely because there are no acid/base groups near His59 N^{ϵ}.) It follows that the second species detected is Cit−Hip, which differs from the Cit−Hie interaction by uptake of a proton. The [6-^{13}C]citrate probe indicates a near-equimolar mixture of Cit−Hie and Cit−Hip configurations, implying that the *Aa*PurE·citrate complex, formed at pH 7.4, was trapped at or near its pK_a. This pH is comparable to the His59-associated pK_a values determined from enzyme velocity studies for free enzyme (7.2 ± 0.1) or the enzyme−CAIR complex (8.4 ± 0.1) (*8*).

ACKNOWLEDGMENT

We thank C. Z. Constantine and T.-Y. Yu for their assistance with REDOR sample preparation.

REFERENCES

1. Mueller, E. J., Meyer, E., Rudolph, J., Davisson, V. J., and Stubbe, J. (1994) N^5-Carboxyaminoimidazole ribonucleotide: Evidence for a new intermediate and two new enzymatic activities in the *de novo* purine biosynthetic pathway of *Escherichia coli*, *Biochemistry 33*, 2269−2278.
2. Kappock, T. J., Ealick, S. E., and Stubbe, J. (2000) Modular evolution of the purine biosynthetic pathway, *Curr. Opin. Chem. Biol. 4*, 567−572.
3. Meyer, E., Kappock, T. J., Osuji, C., and Stubbe, J. (1999) Evidence for the direct transfer of the carboxylate of N^5-carboxyaminoimidazole ribonucleotide (N^5-CAIR) to generate 4-carboxy-5-aminoimidazole ribonucleotide catalyzed by *Escherichia coli* PurE, an N^5-CAIR mutase, *Biochemistry 38*, 3012−3018.
4. Firestine, S. M., Poon, S.-W., Mueller, E. J., Stubbe, J., and Davisson, V. J. (1994) Reactions catalyzed by 5-aminoimidazole ribonucleotide carboxylases from *Escherichia coli* and *Gallus gallus*: A case for divergent catalytic mechanisms, *Biochemistry 33*, 11927−11934.
5. Mathews, I. I., Kappock, T. J., Stubbe, J., and Ealick, S. E. (1999) Crystal structure of *Escherichia coli* PurE, an unusual mutase in the purine biosynthetic pathway, *Struct. Folding Des. 7*, 1395−1406.
6. Settembre, E. C., Chittuluru, J. R., Mill, C. P., Kappock, T. J., and Ealick, S. E. (2004) Acidophilic adaptations in the structure of *Acetobacter aceti* N^5-carboxyaminoimidazole ribonucleotide mutase (PurE), *Acta Crystallogr. D60*, 1753−1760.
7. Hoskins, A. A., Morar, M., Kappock, T. J., Mathews, I. I., Zaugg, J. B., Barder, T. E., Peng, P., Okamoto, A., Ealick, S. E., and Stubbe, J. (2007) N^5-CAIR mutase: Role of a CO_2 binding site and substrate movement in catalysis, *Biochemistry 46*, 2842−2855.
8. Constantine, C. Z., Starks, C. M., Mill, C. P., Ransome, A. E., Karpowicz, S. J., Francois, J. A., Goodman, R. A., and Kappock, T. J. (2006) Biochemical and structural studies of N^5-carboxyami-

noimidazole ribonucleotide mutase (PurE) from the acidophilic bacterium *Acetobacter aceti*, *Biochemistry 45*, 8193−8208.
9. Gullion, T., and Schaefer, J. (1989) Rotational-echo double-resonance NMR, *J. Magn. Reson. 81*, 196−200.
10. Gullion, T., and Schaefer, J. (1989) Measurement of heteronuclear dipolar couplings by MAS NMR, *Adv. Magn. Reson. 13*, 57−83.
11. McDowell, L. M., Schmidt, A., Cohen, E. R., Studelska, D. R., and Schaefer, J. (1996) Structural constraints on the ternary complex of 5-enolpyruvylshikimate-3-phosphate synthase from rotational-echo double-resonance NMR, *J. Mol. Biol. 256*, 160−171.
12. Francois, J. A., Starks, C. M., Sivanuntakorn, S., Jiang, H., Ransome, A. E., Nam, J.-W., Constantine, C. Z., and Kappock, T. J. (2006) Structure of a NADH-insensitive hexameric citrate synthase that resists acid inactivation, *Biochemistry 45*, 13487−13499.
13. Bradford, M. M. (1976) A rapid and sensitive method for the quantitation of microgram quantities of protein utilizing the principle of protein-dye binding, *Anal. Biochem. 72*, 248−254.
14. Stubbe, J. A., and Kenyon, G. L. (1972) Analogs of phosphoenolpyruvate. Substrate specificities of enolase and pyruvate kinase from rabbit muscle, *Biochemistry 11*, 338−345.
15. Schaefer, J., and McKay, R. A. (1999) U.S. Patent 5,861,748.
16. Stueber, D., Mehta, A. K., Chen, Z. Y., Wooley, K. L., and Schaefer, J. (2006) Local order in polycarbonate glasses by $^{13}C\{^{19}F\}$ rotational-echo double-resonance NMR, *J. Polym. Sci., Part B: Polym. Phys. 44*, 2760−2775.
17. Gullion, T., Baker, D. B., and Conradi, M. S. (1990) New, compensated Carr-Purcell sequences, *J. Magn. Reson. 89*, 479−484.
18. Bennett, A. E., Rienstra, C. M., Auger, M., Lakshmi, K. V., and Griffin, R. G. (1995) Heteronuclear decoupling in rotating solids, *J. Chem. Phys. 103*, 6951−6958.
19. Guex, N., and Peitsch, M. C. (1997) SWISS-MODEL and the Swiss-PdbViewer: An environment for comparative protein modeling, *Electrophoresis 18*, 2714−2723.
20. Kraulis, P. J. (1991) Molscript: A program to produce both detailed and schematic plots of protein structures, *J. Appl. Crystallogr. 24*, 946−950.
21. Merritt, E. A., and Bacon, D. J. (1997) Raster3D: Photorealistic molecular graphics, *Methods Enzymol. 277*, 505−524.
22. O'Leary, M. H., Rife, J. E., and Slater, J. D. (1981) Kinetic and isotope effect studies of maize phosphoenolpyruvate carboxylase, *Biochemistry 20*, 7308−7314.
23. Hatch, M. D., and Heldt, H. W. (1985) Synthesis, storage, and stability of [4-^{14}C]oxaloacetic acid, *Anal. Biochem. 145*, 393−397.
24. Li, J., Chatterjee, K., Medek, A., Shalaev, E., and Zografi, G. (2004) Acid-base characteristics of bromophenol blue-citrate buffer systems in the amorphous state, *J. Pharm. Sci. 93*, 697−712.
25. Menzel, U., and Gottschalk, G. (1985) The internal pH of *Acetobacterium wieringae* and *Acetobacter aceti* during growth and production of acetic acid, *Arch. Microbiol. 143*, 47−51.
26. Boyle, M. P., Kalliomaa, A. K., Levdikov, V., Blagova, E., Fogg, M. J., Brannigan, J. A., Wilson, K. S., and Wilkinson, A. J. (2005) Crystal structure of PurE (BA0288) from *Bacillus anthracis* at 1.8 Å resolution, *Proteins 61*, 674−676.
27. Bates, R. G., and Pinching, G. D. (1949) Resolution of the dissociation constants of citric acid at 0 to 50, and determination of certain related thermodynamic functions, *J. Am. Chem. Soc. 71*, 1274−1283.
28. Creighton, T. E. (1983) *Proteins: Structures and Molecular Principles*, W. H. Freeman, New York.
29. Bachovchin, W. W., and Roberts, J. D. (1978) Nitrogen-15 nuclear magnetic resonance spectroscopy. The state of histidine in the catalytic triad of α-lytic protease. Implications for the charge-relay mechanism of peptide-bond cleavage by serine proteases, *J. Am. Chem. Soc. 100*, 8041−8047.
30. Markley, J. L. (1978) Hydrogen bonds in serine proteinases and their complexes with protein proteinase inhibitors. Proton nuclear magnetic resonance studies, *Biochemistry 17*, 4648−4656.
31. Cassidy, C. S., Lin, J., and Frey, P. A. (1997) A new concept for the mechanism of action of chymotrypsin: The role of the low-barrier hydrogen bond, *Biochemistry 36*, 4576−4584.
32. Markley, J. L., Bax, A., Arata, Y., Hilbers, C. W., Kaptein, R., Sykes, B. D., Wright, P. E., and Wuthrich, K. (1998) Recommendations for the presentation of NMR structures of proteins and nucleic acids, *J. Mol. Biol. 280*, 933−952.

BI700899Q